JOURNAL OF MATERIALS SCIENCE **38** (2003) 4895–4903

Grain orientation and anisotropy in the physical properties of $SrBi_2(Nb_{1-x}V_x)_2O_9$ ($0 \leq x \leq 0.3$) ceramics

B. H. VENKATARAMAN, K. B. R. VARMA*
Materials Research Centre, Indian Institute of Science, Bangalore-560012, India
E-mail: kbrvarma@mrc.iisc.ernet.in

$SrBi_2(Nb_{1-x}V_x)_2O_9$ ($0 \leq x \leq 0.3$ in molar ratio) ceramics have been fabricated via conventional sintering at elevated temperatures. Interestingly sintering the pellets in the 1320–1470 K temperature range yielded partially grain oriented ceramics. The orientation factor (f) monitored via X-ray powder diffraction studies was found to increase with increasing V_2O_5 content and reached 83% for $x = 0.3$. The increment in (f) was not that significant with increase in sintering temperature and its duration. The microstructural studies suggest that V_2O_5 has a truncating effect on the abnormal platy growth of SBN grains. The dielectric constant (ε_r) and loss (D) measurements as functions of both temperature and V_2O_5 content have been carried out along the directions parallel (ε_{rp}) and perpendicular (ε_{rn}) to the cold pressing axis of the pellet. The anisotropy ($\varepsilon_{rn}/\varepsilon_{rp}$) associated with ε_r was found to be 1.11 at 300 K and 2.1 at the Curie temperature, (T_c) respectively. Different dielectric mixture formulae that were employed to analyze the effective dielectric constants of these samples with varying porosity confirmed that the experimental value of ε_r was comparable with that obtained using Wiener's formula. Impedance spectroscopy was employed to rationalize the electrical behavior of these ceramics. The pyroelectric coefficients along the directions parallel and perpendicular to the pressing axis of the grain oriented (83%) SBN ceramic at 300 K were 0.13145 mC/m^{2}K and 0.26291 mC/m^{2}K respectively. The ferroelectric properties of these grain-oriented ceramics were better in the direction perpendicular to the pressing axis than those in the parallel direction.

1. Introduction

Ferroelectric materials particularly in thin film geometry belonging to the Aurivillius family of oxides with the general formula $[Bi_2O_2]^{2+}[A_{n-1}B_nO_{3n+1}]^{2-}$ have been on increasing demand owing to their potential applications in a variety of devices which include piezoelectric, pyroelectric and microelectromechanical and non-volatile random access memory (NVRAM) [1–5]. $SrBi_2Nb_2O_9$, (SBN) which is known to be an $n = 2$ member of the above family of layered oxides, has been visualized as a versatile material for multifarious applications. It consists of two perovskite like NbO_6 octahedron units sandwitched between $(Bi_2O_2)^{2+}$ layers along the c-axis and the Sr^{2+} cations are located in the space between these octahedra. It was known that [6] materials with interesting and promising NLO properties could be obtained by substituting Vanadium, the lightest element in group V of the periodic table, for Nb (or) Ta atoms because of the ionic size effects. It was with this motivation, we made attempts to visualize the influence of vanadium doping on the microstructure and physical properties of tungsten bronze type materials such as $K_3Li_2Nb_5O_{15}$ and related compounds [7]. We thought that it is worth attempting to replace Nb (niobium) partially by Vanadium in SBN and study its influence on the microstructural and physical properties. Indeed, Yun Wu *et al*. [8, 9] have reported the effect of the partial replacement of niobium by vanadium on the dielectric and ferroelectric properties of SBN ceramics, when we were in the process of making systematic studies on the influence of vanadium doping on its physical properties. However, to the best of the knowledge of the authors, no systematic reports exist on the effect of vanadium doping on the microstructural aspects of SBN and inturn their influence on the physical properties when these are sintered at elevated temperatures. It is because of the fact that sintering of Bi or V based compounds at higher temperatures but below their decom position temperatures would lead to non-stiochiometry/defect formation (when the Bi or V less are not compensated) and this is expected to influence the microstructure and hence the physical properties.

*Author to whom all correspondence should be addressed.

Indeed interesting results have been obtained by sintering vanadium doped SBN pellets at elevated temperatures (1420 K) and the details of which are elucidated in this paper.

The structural, microstructural, dielectric and ferroelectric properties of SBN ceramics doped with vanadium pentoxide in different concentrations are reported in the following sections.

2. Experimental

Polycrystalline ceramic powders of $SrBi_2(V_xNb_{1-x})_2O_9$ (SBVN) (where $x = 0$, 0.03, 0.05, 0.1, 0.2, and 0.3 designated henceforth as SBN, SBN3, SBN5, SBN10, SBN20 and SBN30 respectively) were prepared by solid state reaction route. Stiochiometric mixture of $SrCO_3$, Bi_2O_3, Nb_2O_5 and V_2O_5 (Aldrich Chemicals) of 99.99% purity was heated in air for 12 h at 1170 K for vanadium doped SBN samples and at 1270 K for the samples without vanadium. The formation of the monophasic compound was confirmed via X-ray powder diffraction (XRD) using Cu K_α radiation. The as-prepared powder was then cold-pressed at 300 K for a few minutes at the pressure of 300 Kg/cm^2. Grain-oriented samples were obtained by subjecting these pressed pellets to the conventional sintering process in air at 1420 K for 10 h. Prior to characterisation and property measurements, all the samples were annealed at 800°C for 3 h in flowing oxygen. The sintered pellets were subjected to XRD studies for the phase identification. The degree of grain orientation (f) was estimated by Lotgering's method [10]

$$f = \left(\frac{P - P_0}{1 - P_0}\right)$$

where $P = \Sigma I_{001}/\Sigma I_{hkl}$ for the given oriented sample and $P_0 = \Sigma I_{001}/\Sigma I_{hkl}$ for the non-oriented sample. The internal strain was calculated by monitoring the line broadening and shift of a few selected peaks.

The densities (ρ) of the sintered pellets were determined by the liquid displacement/Archimedian method. Xylene, the density of which is 0.87 gm/cm^3, was used as the liquid media. The porosity of the pellets was calculated using the relation

$$P = \left(\rho_T - \frac{\rho}{\rho_T}\right)$$

where ρ_T is the theoretical density (7.26 gm/cm^3) for SBN. The microstructural features of the sintered pellets were studied using Scanning Electron Microscopy (SEM) (Leica, 440I, Oxford Instruments).The average grain size was determined from the scanning electron micrograph using the image analysis software (Quantimet MC500) associated with the SEM. The capacitance (C_p) and the dielectric loss (tan δ) measurements were carried out on the polished pellets as a function of the frequency (100 Hz–1 MHz) and temperature (300–770 K), using an impedance analyser (HP 4194A) at a signal strength of 0.5 Vrms. EPR spectroscopy was employed to analyze the valence state of vanadium in SBN at room temperature. The EPR spectra of the samples were obtained on a Varian E109 spectrometer operating in the X-band. The g values were obtained using DPPH as a standard.

The P-E hysteresis loops for vanadium doped SBN ceramics were recorded using a modified Sawyer-Tower circuit [11] at a switching frequency of 50 Hz. The values of remnant polarisation (P_r) and coercive field (E_c) were determined from the hysteresis loops. The pyroelectric coefficients of the present ceramics were measured by Byer and Roundy method [12]. Prior to these measurements the samples were electrically poled with a dc field of 4–5 kV/cm at 500 K and subsequently these were short-circuited to eliminate the surface charge effects. The sample was placed in an oven and ramped at a uniform rate (3°C/min).The pyroelectric current (I) produced parallel to the poling axis owing to the variation of spontaneous polarisation (P_s), with temperature is given by

$$I = A \times P(T)\mathrm{d}T/\mathrm{d}t$$

where $P(T) = \mathrm{d}P_s(T)/\mathrm{d}T$ is the pyroelectric coefficient calculated at a temperature T, A is the electrode area normal to the polar (i.e., poling) axis and $\mathrm{d}T/\mathrm{d}t$ is the heating rate.

3. Results and discussion

3.1. Structural studies and degree of grain-orientation

In Fig. 1a–d, we show the XRD patterns recorded for the randomly oriented polycrystalline SBN10 powder, calcined at 1170 K for 12 h along with those obtained for the faces parallel to the pressing axis of the pellets sintered at 1320 K for different durations (6 h, 10 h, 15 h). In Fig. 1b one would notice the enhanced (008) and (0010) peaks of the ceramic and their intensities increase with increasing sintering duration (Fig. 1c

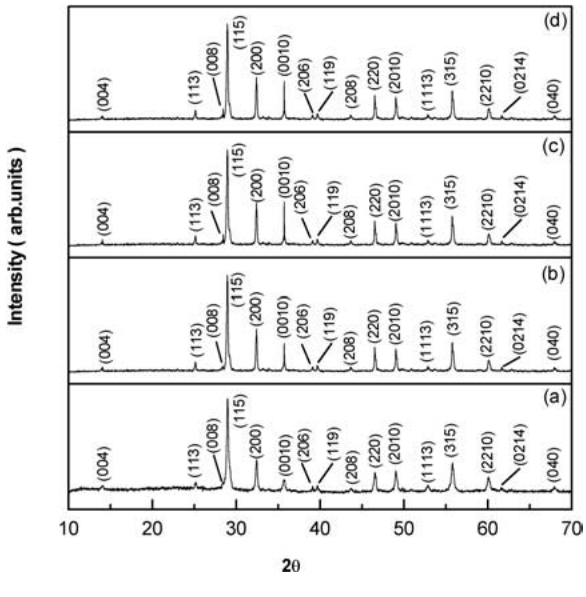

Figure 1 The XRD patterns recorded for the faces parallel to the pressing axis of the SBN10 sample sintered at 1320 K for (b) 6 h, (c) 10 h and (d) 15 h and (a) for randomly oriented as-prepared polycrystalline powder.

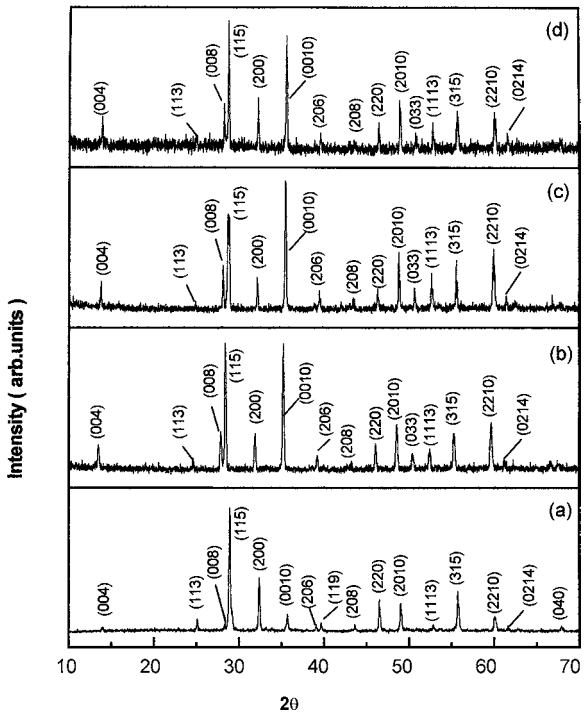

Figure 2 The XRD patterns recorded for the faces parallel to the pressing axis of the SBN10 sample sintered at 1320 K for (b) 6 h, (c) 10 h and (d) 15 h and (a) for randomly oriented as-prepared polycrystalline powder.

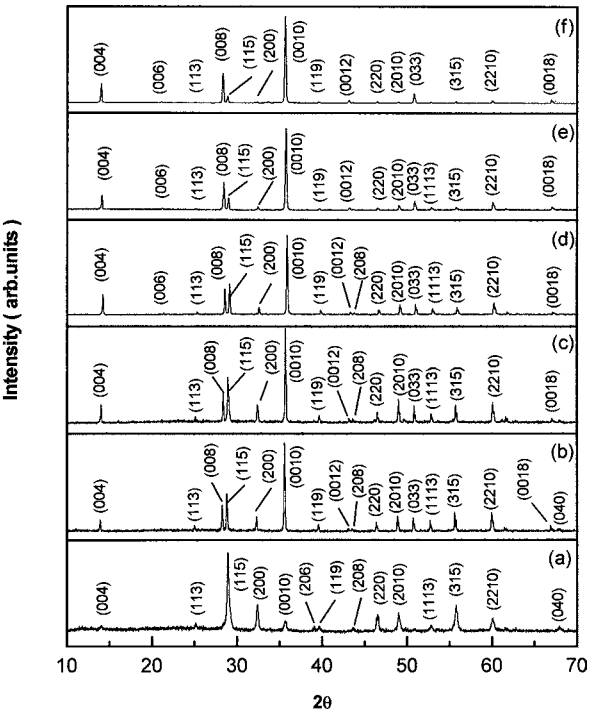

Figure 4 The XRD patterns recorded on the faces parallel to the pressing axis of SBN containing various concentrations of V_2O_5 (b) 3 mol%, (c) 5 mol%, (d) 10 mol%, (e) 20 mol% and (f) 30 mol% and (a) for randomly oriented as-prepared polycrystalline powder.

and d). Further, initial temperatures at which the powdered samples are calcined seem to have a significant effect on the insentisities of (001) peaks. For instance, the starting powders that were calcined at 1270 K for 12 h after pelletizing and sintering at 1320 K for different durations gave rise to enhanced XRD intensities along (004), (008) and (0010), suggesting an increase in orientation factor with increase in initial calcination temperature. Fig. 2b–d, shows the XRD patterns obtained for the faces parallel to the pressing axis of SBN10 sample sintered at 1320 K along with that of the powdered sample (Fig. 2a).The XRD patterns that were obtained for the faces parallel to the pressing axis of the pellets sintered at different temperatures and for the same duration are shown in Fig. 3b–e. The effect of increasing sintering temperature on the orientation of the grains is reflected in increase in intensities of X-ray peaks corresponding to (004), (008) and (0010). Fig. 3a shows the powdered XRD pattern of SBN10 for comparison. However, there is a decreasing tendency in the intensities of (001) peaks for the pellets sintered at 1470 K for 10 h, though no secondary phase is found (Fig. 3e). This implies that no decomposition occurred in the SBN10 sample, unlike SBT ceramic in which a secondary phase was detectable when it was sintered at 1470 K [13].

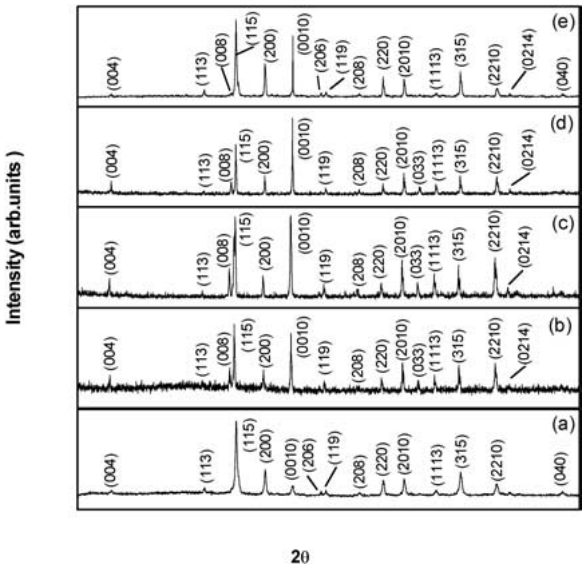

Figure 3 The XRD patterns recorded on the faces parallel to the pressing axis of the SBN10 sample sintered at (b) 1320 K/10 h, (c) 1370 K/10 h, (d) 1420 K/10 h and (e) 1470 K/10 h and (a) for randomly oriented as-prepared polycrystalline SBN powder.

The XRD patterns that were obtained on the faces parallel to the pressing axis of the SBN pellets containing different concentrations of V_2O_5 sintered at 1420 K/10 h are shown in Fig. 4b–f. Also, the XRD pattern obtained for undoped SBN pellet is included in the same figure for comparison (Fig. 4a). The X-ray intensities corresponding to c-planes (i.e.) (004), (006), (008), (0010), (0012) and (0018) have increased with increase in V_2O_5 content. It is interesting to see particularly the peak corresponding to (115) getting reduced in its intensity as the V_2O_5 content increases from 0 to 30 mol%. The XRD patterns recorded on the faces perpendicular to the pressing axis of SBN pellets for various concentrations (3–30 mol%) of V_2O_5 are shown in Fig. 5b–f. We also show the XRD pattern obtained for undoped SBN pellet in Fig. 5a. Though there is an increase in intensity of the peaks corresponding to (200) with increase in V_2O_5 content, it is not that significant. The orientation factor (f) along the parallel

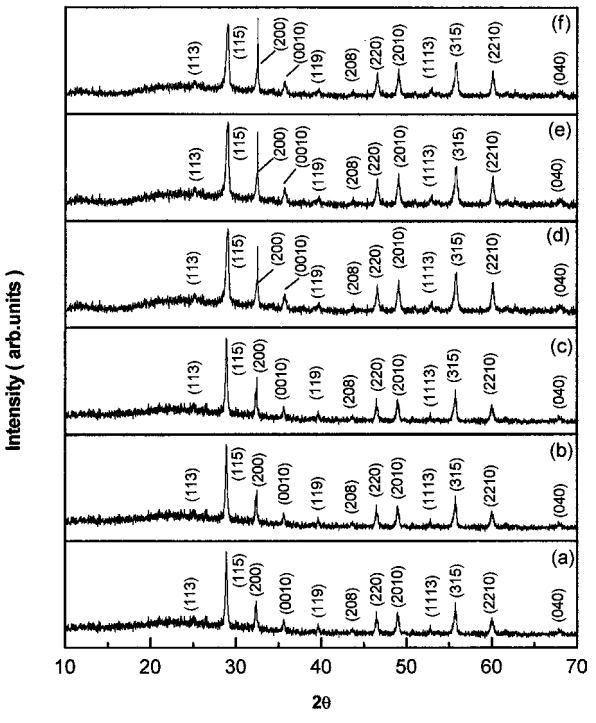

Figure 5 The XRD patterns recorded on the faces perpendicular to the pressing axis of SBN with various concentrations of V_2O_5 (b) 3 mol%, (c) 5 mol%, (d) 10 mol%, (e) 20 mol% and (f) 30 mol% and (a) for randomly oriented as-prepared polycrystalline powder.

direction of the pressing axis increases from 38% to 83% as the V_2O_5 content increases from 3–30 mol% in SBN pellets. In contrast, the orientation factor along the direction perpendicular to the pressing axis increases only from 10% to 23%. The orientation factor (f) associated with these sintered pellets along the parallel and perpendicular faces of the pressing axis is tabulated in the Table I.

3.2. Microstructural analyses

Fig. 6a–c depicts the scanning electron micrographs obtained for the faces parallel to the pressing axis of the as-sintered pellets of SBN, SBN10 and SBN30. The SEM recorded for pure SBN pellets reveal the presence of elongated plate shaped grains associated with inter and intraporosity. In contrast tightly packed plate shaped grains are encountered in the micrographs recorded for SBN10 and SBN30. The plate like morphology is typical of Aurivillius family of oxides and is due to the anisotropic nature of the crystal structure. The c-axis is found to be perpendicular to the major faces of these

TABLE I Grain-orientation factor (f) along the parallel and perpendicular faces of the pressing axis of the V_2O_5 doped SBN

Sl. no.	Sample	Orientation factor (f) parallel to the pressing axis	Orientation factor (f) perpendicular to the pressing axis
1	SBN3	0.38	0.10
2	SBN5	0.44	0.12
3	SBN10	0.54	0.14
4	SBN20	0.71	0.19
5	SBN30	0.83	0.23

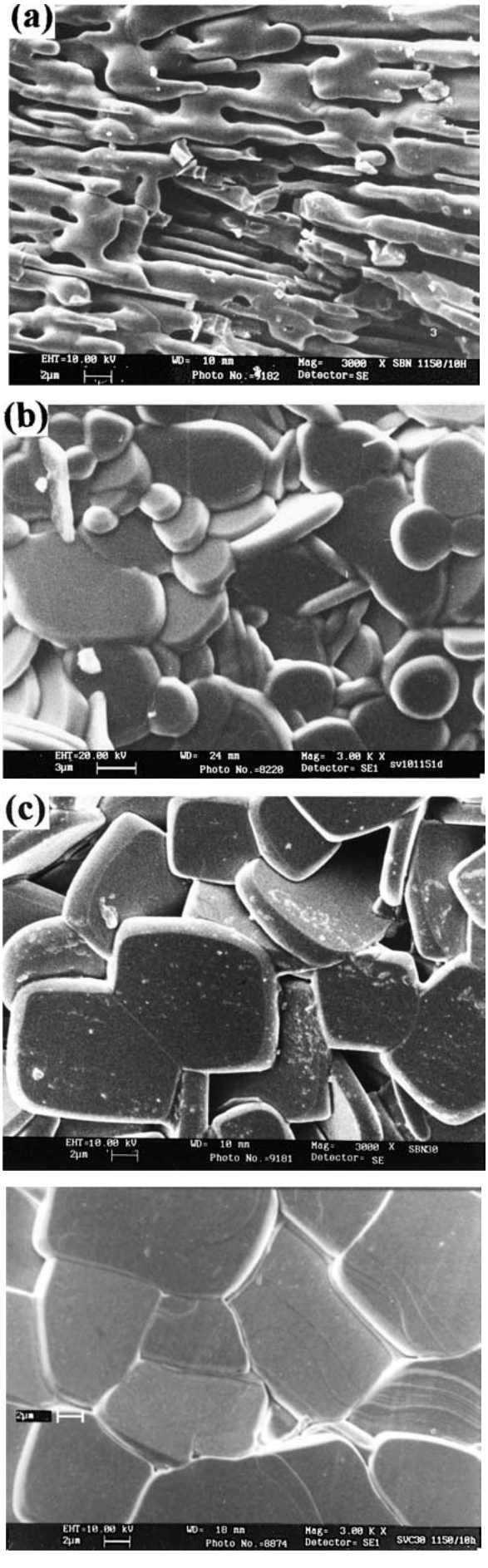

Figure 6 The Scanning Electron Micrographs recorded on the faces parallel to the pressing axis of SBN ceramics containing: (a) no V_2O_5, (b) 10 mol% V_2O_5, (c) 30 mol% V_2O_5, and (d) is for the perpendicular direction to the pressing axis of 30 mol% V_2O_5.

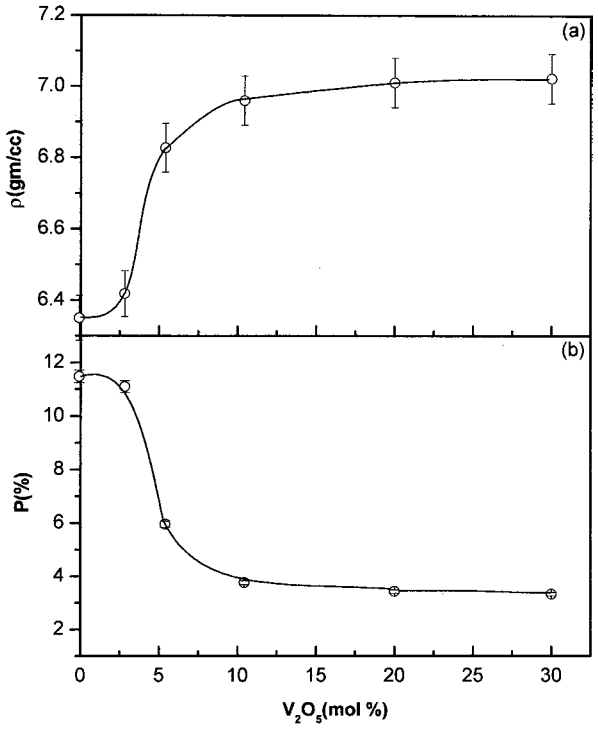

Figure 7 The variation of (a) density and (b) percentage of porosity as a function of V_2O_5 content.

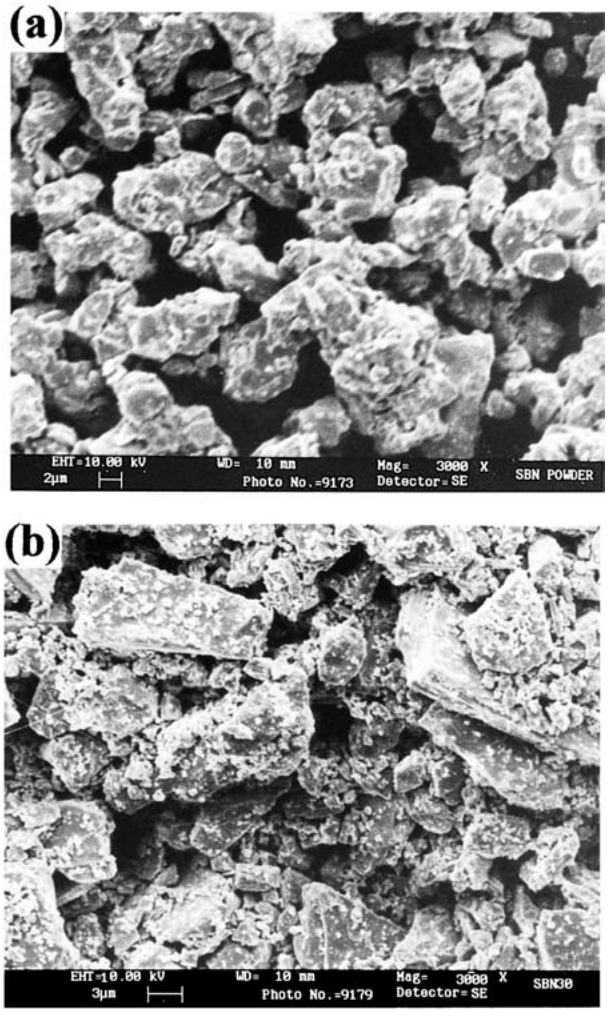

Figure 8 The Scanning Electron Micrographs of the starting SBN powders synthesized: (a) without V_2O_5 and (b) with 30 mol% V_2O_5.

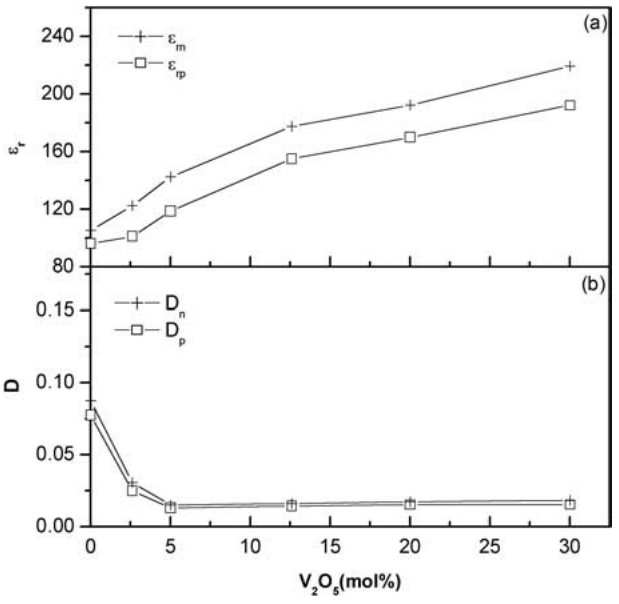

Figure 9 The variation of (a) ε_{rn} and ε_{rp} and (b) D_n and D_p, (at 100 kHz) as a function of the concentration of V_2O_5 in SBN at 300 K.

grains showing a preferential orientation in XRD pattern [13]. The grain size is found to increase with increase in V_2O_5 content. The transformation that is encountered in the morphological features of the grains is attributed to the slight amount of liquid phase that is provided by the presence of V_2O_5 and non-stiochiometry arose as a result of sintering these pellets at elevated temperatures. We believe that excess V_2O_5 that is likely to segregate at the grain boundaries has facilitated the plate shaped grain growth and effective packing via liquid phase sintering. However, the grain growth along the perpendicular direction which is the polar direction (a or b) is slightly higher than the parallel direction of the pressing axis. For the sake of comparison we have shown the microstructure recorded for the face perpendicular to the pressing axis of the SBN30 sample (Fig. 6d). These results are akin to those reported for the other layered bismuth containing compounds [14–16]. The experimental density and the percentage of porosity of the samples (SBN-SBN30) are shown in Fig. 7a and b. Increase in V_2O_5 content resulted in obtaining dense ceramics and uniform microstructure.

Most of the layered perovskites were known to exhibit preferential grain growth along the *c*-direction. As indicated earlier, the enhanced grain growth and effective packing of SBN grains along the pressing axis is believed to be due to the small amount of the liquid phase formation of the impurity phase present at the grain boundary during sintering. Fig. 8a and b shows the SEM images recorded on the starting powders of undoped SBN and SBN30 samples. These indicate that the vanadium doped SBN particles are non-spherical to begin with itself. Since the starting particles are non-spherical, one would expect an anisotropy in the pore structure and grain boundary energy, which would lead to the observed grain-orientation.

The densification parallel to the pressing axis which appears to be different from that of the normal one is due to the particle rearrangement in the initial stage of the sintering of the non-spherical powder. The driving force

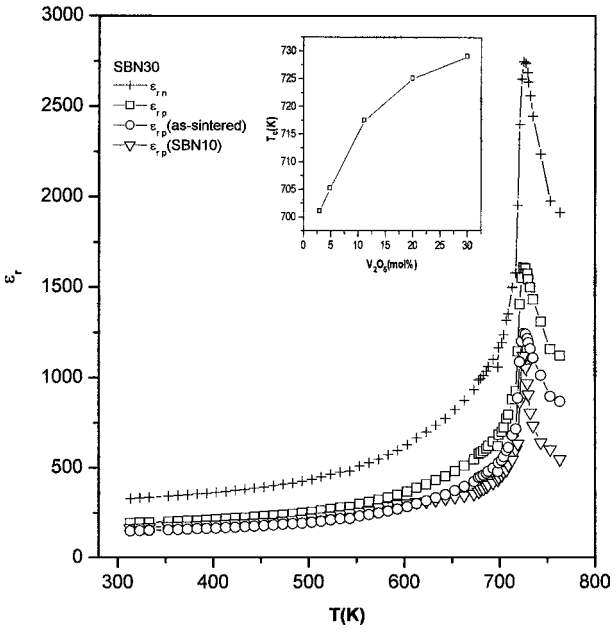

Figure 10 The temperature dependence of ε_r (at 100 kHz) along the direction parallel (ε_{rp}) to the pressing axis for the 10 mol%, 30 mol% V_2O_5 doped SBN samples along with that of the dielectric constant measured for as-sintered and also for the perpendicular (ε_{rp}) direction to the pressing axis. Inset shows the variation of T_c with V_2O_5 content.

for densification is derived from the capillary pressure of the liquid phase located between the fine solid particles. The laplacian force gives rise to a strong attractive force between the neighbouring particles. The origin of the attractive force is from the component of the liquid/vapour surface energy (γ_{lv}) normal to the two surfaces. Since the surface free energy of the layered perovskite is minimum along the *c*-axis, the capillary pressure will tend to rearrange the solid particles of the doped SBN sample so as to give maximum packing and a minimum of resultant pore surface along the

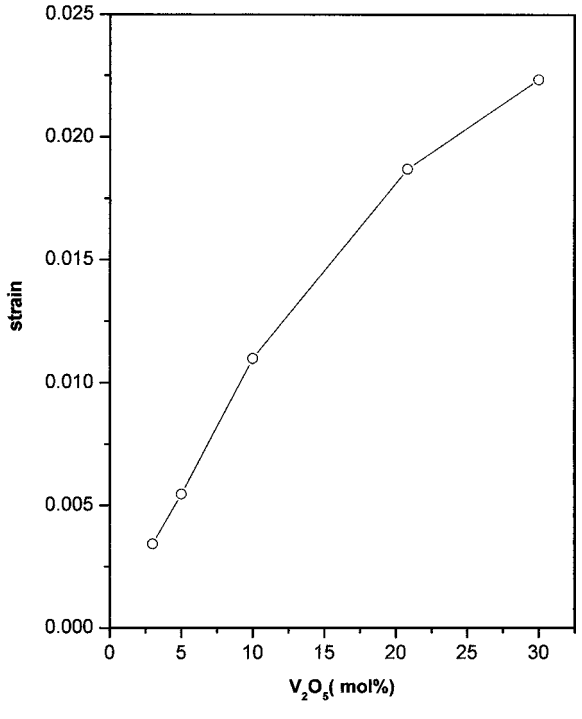

Figure 11 Variation of internal strain as a function of V_2O_5 content.

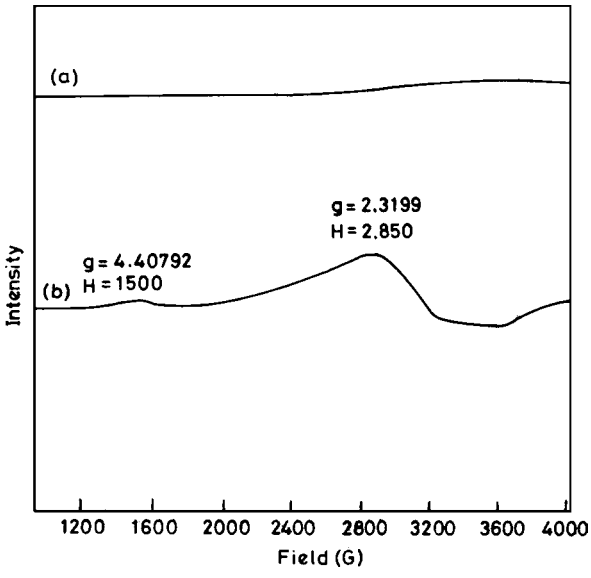

Figure 12 EPR spectra for the as-sintered and oxygen annealed 30 mol% V_2O_5 doped SBN sample.

pressing axis during the initial stage of the sintering. This results in an enhanced grain orientation along the pressing axis as compared to that of the normal one. The grain orientation in the direction perpendicular to the pressing axis of the doped SBN sample is inhibited by the pores, located at the grain boundaries and remain open until the later stage of sintering [17]. The microstructures recorded on the parallel and perpendicular faces of the pressing axis of the representative SBN30 sample which are shown in Fig. 6c and d corroborate the above argument.

3.3. Dielectric studies

The dielectric constant (ε_r) and dielectric loss (D) measured as a function of V_2O_5 content at room temperature, along the parallel (ε_{rp} and D_p) and the normal (ε_{rn} and D_n) directions to the pressing axis are shown in Fig. 9a and b. There exists a clear dielectric anisotropy over the entire range of the compositions attempted in the present investigations. The dielectric constant measured along the direction perpendicular (*a*-axis) to the pressing axis is higher than the one measured parallel to the pressing axis at 100 kHz .The dielectric loss of the SBN doped V_2O_5 samples are lower than that of the undoped samples. The anisotropy in the dielectric loss of doped SBN samples is not very significant. However, the increase in the dielectric constant with increase in V_2O_5 content in both the directions is noteworthy.

Fig. 10 shows the temperature dependence of ε_r measured for SBN10 and SBN30 along the direction parallel to the pressing axis, along with that of the dielectric constant measured along the direction perpendicular to the pressing axis of the SBN30. Also, the variation of ε_r with temperature for as-sintered SBN30 is included in the same figure. The variation of the dielectric loss with temperature is consistent with that of the dielectric data (which is not shown here). The V_2O_5 doped sample has higher ε_r not only at room temperature, but also in the vicinity of the Curie temperature (T_c) and

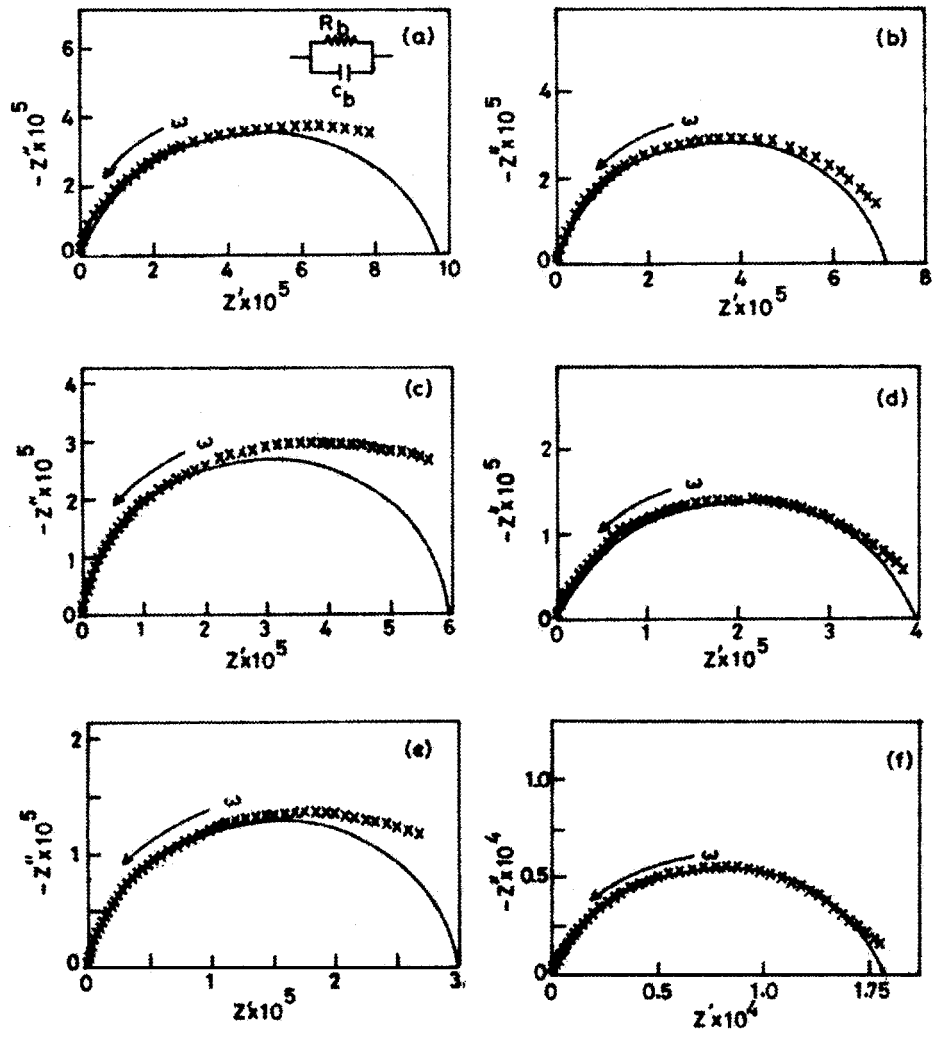

Figure 13 Impendance plots obtained for (a) without V_2O_5, (b) 5 mol%, (c) 10 mol%, (d) 20 mol% (e) 30 mol% V_2O_5 along the direction parallel to the pressing axis of SBN ceramics at 670 K and (f) for the 30 mol% V_2O_5 along the direction perpendicular to the pressing axis at 670 K.

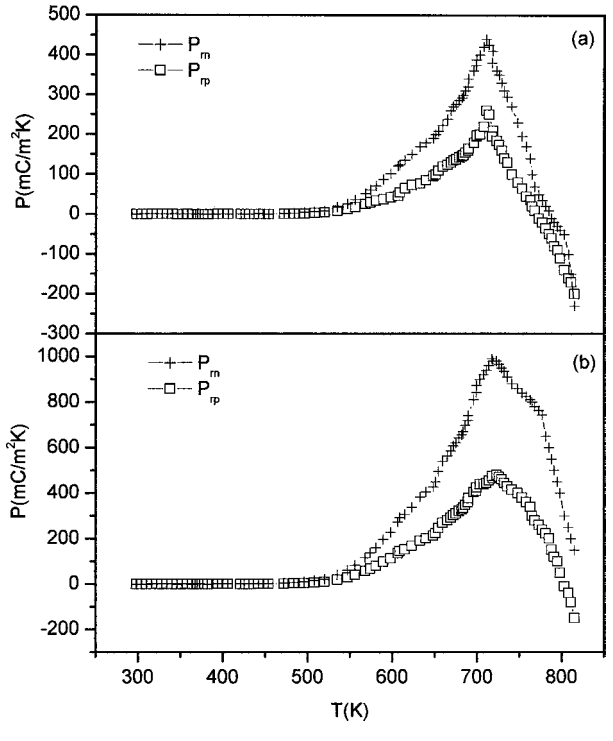

Figure 14 Variation of the pyroelectric coefficient with temperature along the direction parallel and perpendicular to the pressing axis for (a) 10 mol% and (b) 30 mol% V_2O_5 containing SBN ceramics.

above. The dielectric constant increases gradually with increase in temperature up to about 600 K, and subsequently there is a rapid increase and exhibits peaks at 720 and 730 K for SBN10 and SBN30 samples respectively. The Curie temperature gradually increases (700–730 K) with increasing V_2O_5 content and is shown as the inset in Fig. 10. The shift in the T_c may be attributed to the increase in the strain with increase in V_2O_5 content. The lattice strain was calculated based on X-ray line broadening method [18]. A plot of $\beta \cos\theta$ vs. $\sin\theta$ was generated and the strain involved has been calculated based on the slope obtained. Here, $\beta = \Delta\theta_c + \Delta\theta$, and $\Delta\theta_c$ is the full width at half maximum (FWHM) of the peak at the Bragg angle θ (radians) and $\Delta\theta$ is the shift in the peak position. The (008), (115) and (0010) peaks were considered for these calculations. Fig. 11 shows that the variation of internal strain with increasing vanadium content. The increase in strain could have dilation effect on the lattice implying an increase in the lattice parameter a or c. Indeed we did observe an increase in the lattice parameter a with increase in V_2O_5 content. The upward shift in the T_c is attributed to the dilation effect that is brought about by the presence of V_2O_5 in the lattice.

The ε_{rn} values are higher than ε_{rp} values both at 300 K and in the vicinity of T_c for the SBN30 sample

suggesting that the polar axis lies in the ab-plane. Therefore, the dielectric constant along any axis in the ab-plane is expected to be higher than that measured normal to the ab-plane. In the grain-oriented ceramics, since most grains are aligned with their *c*-axes along the pressing direction, the dielectric constant measured along the direction perpendicular to the pressing axis is higher. The oxygen annealed sample shows higher dielectric constant than that of the one sintered in air. The higher ε_r for oxygen annealed ceramic is attributed to the presence of V^{5+} ions in the ceramics. EPR studies carried out on the samples heat treated only in air confirmed the presence of V^{4+} ions. Fig. 12a and b shows the EPR spectra recorded for the as-sintered and oxygen annealed SBN30 sample. EPR spectra of the as-sintered sample is characterized by two asymmetric peaks. These are characteristics of V^{4+} ions in dipolar interaction with other V^{4+} ions [19]. On the other hand, the oxygen annealed sample does not show any peak, indicating the absence of V^{4+} ions. The effect of oxygen annealing, transformed V^{4+} ions into V^{5+} accompanied by a reduction in the ionic size with an increased rattling space which gave rise to higher polarizability. This led to the higher dielectric constant.

These pentavalent vanadium ions are stabilized by oxygen annealing and thus no appreciable oxygen vacancies exist which would lead to a decrease in the dielectric loss, *D*.

3.4. Impedance analysis

Electrical transport properties of the polycrystalline ceramics are known to be strongly effected by their microstructures. Impedance spectra, which accurately reflect the microstructural features are employed to analyze the electrical properties.

Fig. 13a–e shows the impedance plots obtained for the samples (SBN-SBN30) along the direction parallel to the pressing axis. The semicircles that are obtained in the frequency range covered (100 Hz–40 MHz) in the present study suggest that the contribution to the observed values originates from the grain interior. The

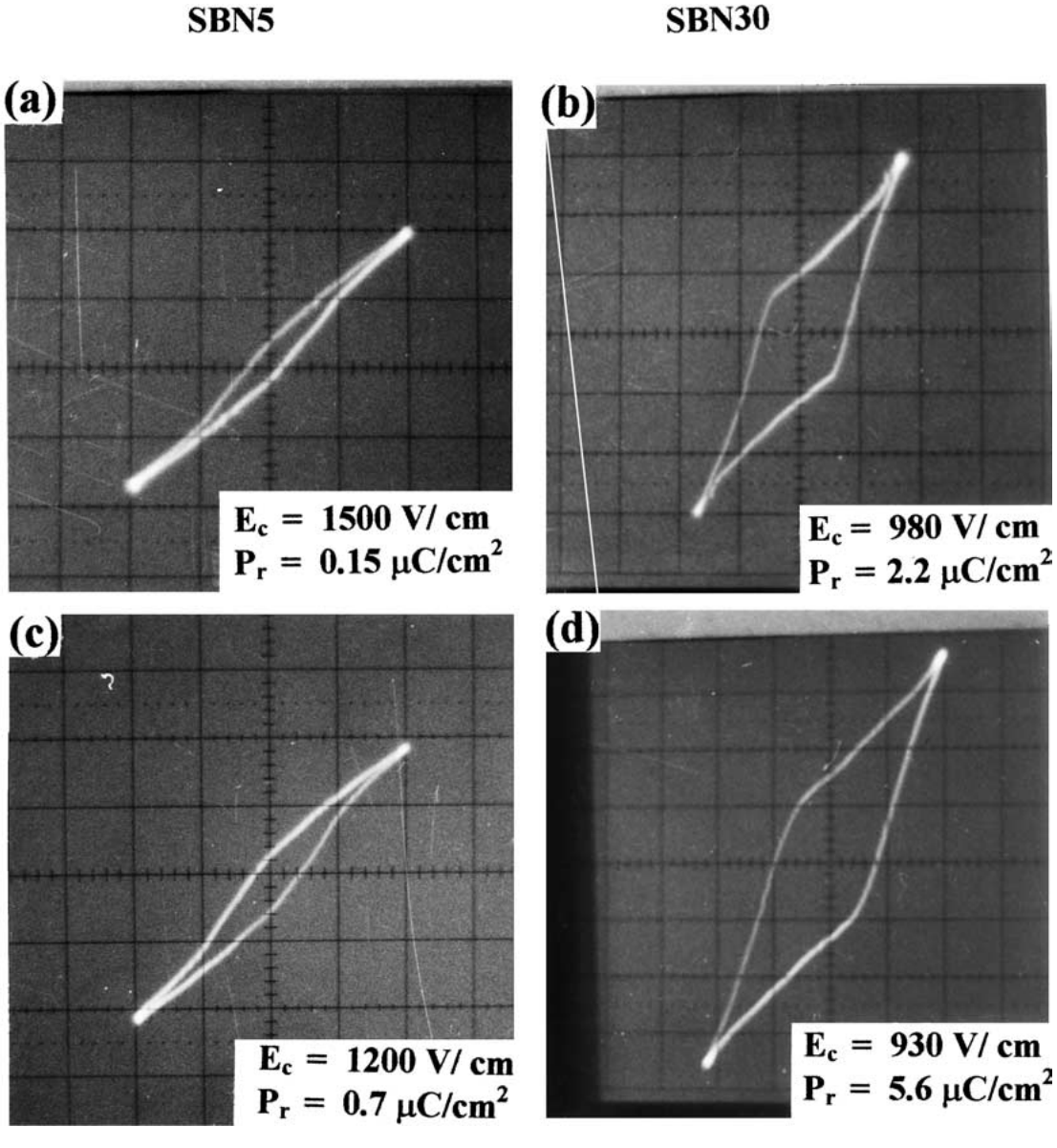

Figure 15 The *P* vs. *E* hysteresis loops for the SBN5 and SBN30 samples, recorded with the switching field applied in the direction parallel (a) and (b) and perpendicular (c) and (d) to the pressing axis at 670 K.

TABLE II Relaxation frequency (f_o), bulk resistance (R_b) and bulk capacitance (C_b) of the grain-oriented samples along both the directions

Sl. no.	Sample	Measured along the direction	f_o (Hz)	R_b (ohm)	C_b (Farad)
1	SBN3	Parallel	2682	9.7×10^5	0.6×10^{-11}
2	SBN5	Parallel	1407.41	7.15×10^5	1.5×10^{-10}
3	SBN10	Parallel	800.14	5.96×10^5	3.3×10^{-10}
4	SBN20	Parallel	319.29	3.97×10^5	13×10^{-10}
5	SBN30	Parallel	316.22	3.74×10^5	16×10^{-10}
6	SBN30	Perpendicular	400.43	1.57×10^4	253×10^{-10}

effects due to the grain boundary and the electrode in the range of frequencies studied are obscure. The equivalent electrical circuit of these samples could be regarded as a single RC combination. On the other hand measurements made along the direction perpendicular to the pressing axis for the SBN30 sample shows the resistance of the grain to be lower by one order of magnitude (Fig. 15f). The bulk capacitance is higher along the perpendicular direction, accounting for higher ε_r along that direction. The values of bulk resistance (R_b), bulk capacitance (C_b) and maximum frequency (f_o) through which the semicircle passes in both the directions are listed in Table II.

3.5. Pyroelectric properties

The pyroelectric measurements were carried out on the grain-oriented samples in the parallel (P_{rp}) and the perpendicular (P_{rn}) directions. Fig. 14a and b depicts the temperature dependence of the pyroelectric coefficient (P) measured in the two directions for the samples SBN10, SBN30. The anisotropy (P_{rn}/P_{rp}) that was found for the SBN10 and SBN30 samples was 1.73 and 2.0 respectively. In both the directions of these samples, P is positive and exhibits a peak near T_c (714 K and 722 K), and subsequently decreases and attains negative sign. The positive sign of P prior to T_c indicates that P_{sec}, which is piezoelectric in origin is larger than P_{pri} in the temperature range (300–870 K) studied.

3.6. Ferroelectric properties

The P vs. E hysteresis loops for the grain oriented samples (SBN5 and SBN30) recorded with the switching field applied in the direction parallel and perpendicular to the pressing axis are shown in the Fig. 15a–d. The loops were recorded in both the directions at 670 K. The values of remnant polarisation (P_r) are higher along the perpendicular direction than that of the parallel direction for SBN5 and SBN30, suggesting that the polar axis lies in the c-plane (a or b-axis). On the other hand, the values of coercive field (E_c) as expected are higher along the parallel direction for both the samples, indicating that a large field is required to switch the spontaneous polarisation along the c-axis.

4. Conclusions

Grain-oriented (83%) ceramics of vanadium doped strontium bismuth niobate were fabricated via cold pressing followed by conventional sintering at 1420 K. The strong preferential orientation of the grains varies with increase in V_2O_5 content. The average grain size of these ceramics increases with increasing V_2O_5 content. Significant anisotropy in the dielectric constant ($\varepsilon_{rn}/\varepsilon_{rp} = 1.11$ at 300 K and 2.1 at T_c) was found in the sample which had the highest orientation factor. The experimental values of the dielectric constants of these ceramics were computed with those obtained using various dielectric mixture formulae. These results were found to be in agreement with those predicted by Wiener's model. The grain capacitance obtained by the complex impedance analyses is higher along the perpendicular direction of the SBN30, which accounted for the incidence of higher dielectric constant. The pyroelectric coefficient was higher along the perpendicular direction than that obtained in the parallel direction. Higher P_r and lower coercive field E_c were found in the direction perpendicular to the pressing axis of V_2O_5 doped SBN ceramics.

Acknowledgements

The authors thank the Department of Science and Technology (DST) for financial grant. We also acknowledge Mr. Vynatheya for his help in carrying out scanning electron microscopy.

References

1. S. DEY and R. ZULEEG, *Ferroelectrics* **108** (1990) 37.
2. J. F. SCOTT and C. A. PAZ DE ARAUJO, *Science* **246** (1989) 1400.
3. G. H. HAERTLING, *J. Vac. Sci. Techol.* **9** (1990) 414.
4. J. J. LEE, C. L. THIO and S. B. DESU, *J. Appl. Phys.* **78** (1995) 5073.
5. H. N. AL-SHAREEF, A. I. KINGON, X. CHEN, K. R. BELLUR and O. AUCIELLO, *J. Mater. Res.* **9** (1994) 2986.
6. R. S. FEIGELSON, G. W. MARTIN and B. C. JOHNSON, *J. Cryst. Growth* **13/14** (1972) 686.
7. K. V. R. PRASAD, S. PHILIP and K. B. R. VARMA, *J. Mater. Sci. Lett.* **12** (1993) 1871.
8. YUN WU and GUOZHONG CAO, *Appl. Phys. Letts.* **75** (1999) 2650.
9. *Idem.*, *J. Mater. Res.* **15** (2000) 1583.
10. F. K. LOTGERING, *J. Inorg. Nucl. Chem.* **9** (1959) 113.
11. C. B. SAWYER and C. H. TOWER, *Phys. Rev.* **35** (1930) 269.
12. R. L. BYER and C. B. ROUNDY, *Ferroelectrics* **3** (1972) 333.
13. YI-CHOU CHEN and CHUNG-HSIN LU, *Integr. Ferroelec.* **26** (1999) 65.
14. K. SAKATA, T. TAKENAKA and K. SHOJI, *Ferroelectrics* **22** (1978) 825.
15. T. KIMURA, M. H. HOLMES and R. E. NEWNHAM, *J. Amer. Ceram. Soc.* **65** (1982) 223.
16. V. N. SIGAEV, E. V. LOPATINA, P. D. SARKISOV, S. YU. STEFANOVICH and V. I. MOLEV, *Mater. Sci. Engg.* B **48** (1997) 254.
17. T. YAMAGUCHI and H. KOSHA, *J. Amer. Ceram. Soc.* **64**(5) (1981) C84; **66**(3) (1983) 210.
18. K. GURUMURUGAN, D. MANGALARAJ, SA. K. NARAYANDASS, K. SEKAR and C. P. GIRIJA VALLABHAN, *Semicond. Sci. Technol.* **9** (1994) 1.
19. A. ABOUKAIS, F. DELMAIRE, M. RIGOLE, R. HUBANT and G. MAIRESSE, *Chem. Mater.* **5** (1993) 1819.
20. H. FROLICH, "Theory of Dielectrics" (Clarendon Press, Oxford, 1949).
21. K. LICHTENECKER, *Phys. Zeitsch.* **27** (1926) 115.
22. N. WIENER, *ibid.* **5** (1904) 332.
23. *Idem.*, *Leipzig* **61** (1909) 113.

Received 2 January
and accepted 18 August 2003